Binarization filtering algorithm for visual image processing of mine inspection robot

This paper mainly aimed at the risk factors such as rock cracking in the process of mining operations, the use of a visual warning function of inspection robot instead of manual inspection operations. The inspection robot body module and the three joint robot arm and the telescopic boom structure can be moved on the steel cord which is laid along the mine overhead line, and the dynamic model of the inspection robot is determined. The robot vision system to detect mine tunnel crack images collected through the camera inspection robot for visual processing using the improved Otsu algorithm for gray-scale image binarization can improve the effect of image processing.

Key words: Robot; dynamics model; image binarization; improved Otsu algorithm

1. Introduction

In coal mine underground work mainly exist in the process of rock bursts, the unsafe factors including of gas and in the event of danger consequence is very serious (Guo and Wang, 2012; Guo and Hong,2005). Due to gas and impact ground pressure before the formation of sudden accident, will show the signs, such as rock burst, etc., in order to eliminate unsafe factors as early as possible and improve the safety of production, daily patrol prevention is particularly important (Guo and Wang, 2012).

But work under the mine dust, air penetrability is not high, poor illumination, unfavourable to patrol and inspection personnel find problems in time (Gong, 2002), at the same time is artificial patrol the problem such as the intensity of labour and the line of sight is not good (Ranjan,Mukheijee and Yoshihiko, 2012). To this end, this paper studied a mining steel rope inspection robot (Ranjan,Mukheijee and Yoshihiko, 2012), can take the place of inspection personnel of mine tunnel rock crack monitoring work (Shriram, 2011; Xue and Li, 2010).

Inspection robot to transmit the camera back after image processing can monitor the mine rock and early warning of dangerous situation and conditions for continuous monitoring of the mining (Zhou and Li, 2006), facilitate early detection of an aura, corresponding prevention measures should be taken to prevent the significant loss of equipment and personnel.

Mr. Shuangming Ling, School of Mechanic, Changsha Aeronautical Vocational and Technical College, Hunan 410 124, China

2. Introduction of mine inspection robot

The robot has some difficulties in the development of the robot in the field of underground dust, bad condition, electromagnetic interference and unstructured operation environment. First, due to the complexity of the underground structure, high flexibility, robot walking on the wire requires a high reliable motion mechanism, to ensure the normal work of the robot. Second, the line inspection robot in a large range of underground long time work needs to be battery powered, sustained and long-term power supply to provide protection for the power of the robot. Third, the robot needs to image processing of the image of the rock early warning, which requires a high visual ability of the robot. Fourth, autonomous behaviour control and navigation complex non-structured environment of the inspection robot. Fifth, robot remote communication, monitoring and remote operation in the mine under harsh conditions are under strong electromagnetic interference normal distance. Finally, it is the special protection mechanism of the ontology in the dangerous work environment. In order to solve the above problems, referring to the research results of domestic and international inspection robot, based on Hunan University developed robot system, mine inspection robot was improved after the basic structure and functions are shown in Fig.1.

3.The dynamic model of the robot for the inspection of the mine

3.1. Dynamic analysis of mine inspection robot

In this paper, the Lagrange method is used to model the dynamic model of the inspection robot. The inspection robot cabin suspended, composed of two joint mechanical arm and three telescopic arm movement to the mobile robot body and adjust the position, when the mobile work laid along the mine steel rope overhead effect, due to the motion of the arm to produce reaction force and torque on the body, it cannot solve the problem of robot kinematics only taking into account the inspection robot for special and complex working environment. The following is the specific method of dynamic

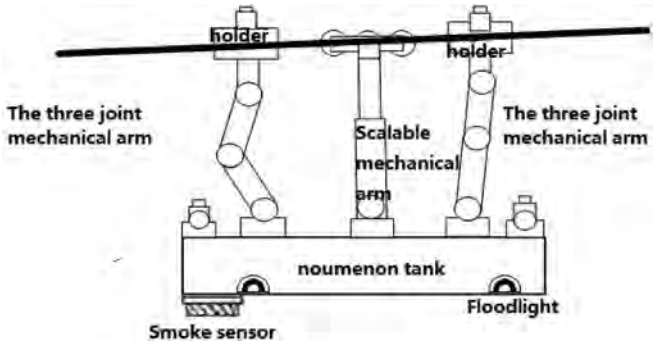

Fig. 1 The basic structure of the inspection robot

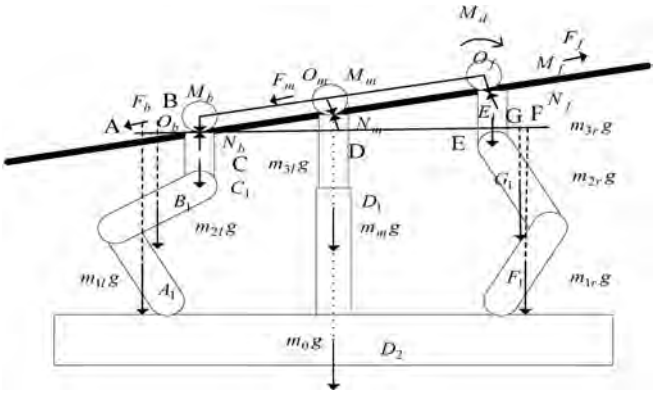

Fig.2 Dynamic model of inspection robot

modeling of inspection robot (Fig.2).

The mechanical analysis of the Y direction (vertical) includes:

$$N_b + N_m + N_f - mg\cos\alpha = 0 \quad \text{...} \quad (1)$$

$$M_b - \delta N_b = 0 \quad \text{...} \quad (2)$$

$$M_m - \delta N_m = 0 \quad \text{...} \quad (3)$$

$$M_f - \delta N_f = 0 \quad \text{...} \quad (4)$$

In the formula, N_b, N_m, N_f are revolver, middle wheel and the right wheel pressure; M_b, M_m, M_f are a right wheel, a middle wheel, a bearing friction moment of couple; g is the weight acceleration; d is the coefficient of friction; $m = \sum_{i=1}^{3} m_{ir} + \sum_{i=1}^{3} m_{il} + m_0 + m_m$ represents the total quality.

Then the mechanical analysis of the X direction (horizontal) included:

$$F_f + F_m - F_b - mg\sin\alpha - ma = 0 \quad \text{...} \quad (5)$$

$$M_d - M_f - F_f r = 0 \quad \text{...} \quad (6)$$

$$M_m - F_m r = 0 \quad \text{...} \quad (7)$$

$$M_f - F_f r = 0 \quad \text{...} \quad (8)$$

In the formula, M_d represents revolver drive motor torque; r represents stress wheel radius; a represents the inspection robot crawling acceleration.

Then analyzes the inspection robot torque sum:

$$M_d + M_g + M_b + M_m + M_f - N_f d_2 - N_m d_1 = 0 \quad \text{...} \quad (9)$$

The gravity effect of the driving device need not to calculate, and the total potential energy of the inspection robot system is:

$$p \approx \sum_{i=1}^{3} p_i = -\sum_{i=1}^{3} m_i \vec{g}^{\,T} T_i \vec{r}_i \quad \text{...} \quad (10)$$

So, using the Lagrange method to solve the dynamic equation of the inspection robot inertia coefficient, the radial force and the force coefficient, the inertia coefficient, the radial force and the force coefficient are calculated separately.

They are:

$$D_{11} = m_1 + m_2 + m_3 + I_{a1}$$

$$D_{22} = I_{2xx} + I_{2yy} + c_3^2 I_{3xx} + s_3^2 I_{3yy} + I_{3zz} + m_3 l$$

$$D_{33} = I_{3xx} + I_{3yy}$$

$$D_{12} = m_2 \bar{y}_2 s_2 - m_3 l s_2$$

$$D_{122} = c_2 m_2 \bar{y}_2 - c_2 l m_3$$

$$D_{222} = s_2 c_2 I_{2y}$$

3.2. Kinematic and dynamic mixed model of inspection robot

The intermediate inspection robot arm can be stabilized, so the wire rope can save underground counterforce to the inspection robot body regardless of centroid, the centroid offset ontology robot system does not exist Y angle and X direction. In the process of inspection robot, the middle arm is included in the model of the robot body in the robot body. Therefore, the hybrid model of the inspection robot is equivalent to the following Fig.3.

According to the method of solving the system of mass center of mass:

$$m_0 r_0 + \sum_{i=1}^{3} m_{il} r_{il} + \sum_{i=1}^{3} m_{ir} r_{ir} = f(\phi_0\ \ \phi_{ij} \quad \text{...} \quad (11)$$

Because the middle arm can play a stabilizing role, this paper can be drawn: $f(\phi_0, \phi_{ij}) = 0$. When the robot arm is rotated about the center axis of the robot system, it satisfies the Euler equation:

$$I_0\omega_0 + m_0 r_0 \times \dot{r}_0 + \sum_{i=1}^{3} (I_{ir}\omega_{ir} + m_{ir} r_{ir} \times \dot{r}_{ir})$$

$$+\sum_{i=1}^{3}(I_{il}\omega_{il}+m_{il}r_{il}\times\dot{r}_{il})=F(\phi_0,\phi_{ij}) \quad \text{... (12)}$$

$$F(\phi_0,\phi_{ij})=\begin{bmatrix} I_{a1}(\omega_{1l}+\omega_{1r}) \\ (I_{2xx}+I_{2yy}+c_3^2I_{3xx}+s_3^2I_{3yy}+I_{3zz})*(\omega_{2l}+\omega_{2r}) \\ (I_{3xx}+I_{3zz})*(\omega_{3l}+\omega_{3r}) \end{bmatrix} \quad \text{... (13)}$$

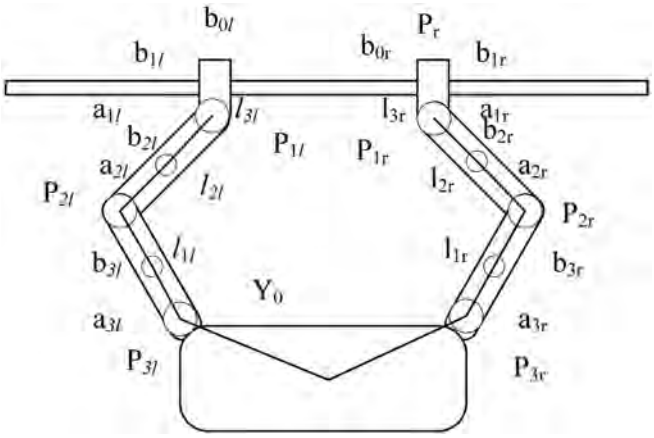

Fig.3 Equivalent diagram of the hybrid model of the inspection robot

$F(\phi_0,\phi_{ij})$ is the momentum and momentum vector of the whole robot system in the inertial coordinate system. According to the geometric relationship between the connecting rod:

$$r_{ir}-r_{(i-1)r}=a_{ir}-b_{(i-1)r},\ i \quad 1,2,3 \quad \text{... (14)}$$

$$r_{il}-r_{(i-1)l}=a_{il}-b_{(i-1)l},\ i \quad 1,2,3 \quad \text{... (15)}$$

Geometric characteristic equation of robot system:

$$P_r=r_0+b_{0r}+\sum_{i=1}^{3}l_{ir}=\sum_{i=0}^{7}k_i^r\begin{bmatrix}C_i\\S_i\\\varphi_i\end{bmatrix},\ i \quad 1,2,3 \quad \text{... (16)}$$

$$P_l=r_0+b_{0l}+\sum_{i=1}^{3}l_{il}=\sum_{i=0}^{7}k_i^l\begin{bmatrix}C_i\\S_i\\\varphi_i\end{bmatrix},\ i \quad 1,2,3 \quad \text{... (17)}$$

Both k_i^r and k_i^l are determined by the geometric structure of the inspection robot,

$$m=m_0+\sum_{i=1}^{3}m_{il}+\sum_{i=1}^{3}m_{ir},\ m^r=\sum_{i=1}^{3}m_{ir},\ m^l=\sum_{i=1}^{3}m_{il},$$

according to (13), (14), (15), (16), (17), after transformation can obtain:

$$P=\begin{bmatrix}P_r\\P_l\end{bmatrix}=\begin{bmatrix}\sum_{i=0}^{7}k_i^rC_i\\\sum_{i=0}^{7}k_i^rS_i\\\sum_{i=0}^{7}k_i^lC_i\\\sum_{i=0}^{7}k_i^lS_i\end{bmatrix} \quad \text{... (18)}$$

On both sides of time derivative:

$$\dot{P}=\begin{bmatrix}\dot{P}_r\\\dot{P}_l\end{bmatrix}=J_s\dot{\phi}_0+J_m\dot{\phi}_m \quad \text{... (19)}$$

J_s represents the relationship between the angular velocity of the body and the velocity of the end effector, and J_m represents the relationship between the angular velocity of each joint and the velocity of the end effector. The $\dot{P}$ represents the end of the manipulator, $\dot{\phi}_m=[\dot{\phi}_{1r},\dot{\phi}_{2r},\dot{\phi}_{3r},\dot{\phi}_{1l},\dot{\phi}_{2l},\dot{\phi}_{3l}]^T$ represents the angular velocity of each joint.

The same as above, the position vector of the center of mass of no. j connecting rod of the robot's no. i manipulator is r_{ij} (i = 1, 2, 3, j = l, r) in the inertial coordinate system, and the position vector of the mass center of the body in the inertial coordinate system is r_0.

$$r_0=\sum_{n=0}^{7}X_{0n}\begin{bmatrix}C_n\\S_n\end{bmatrix},\quad r_{ir}=\sum_{n=0}^{7}Y_{in}\begin{bmatrix}C_n\\S_n\end{bmatrix},$$

$$r_{il}=\sum_{n=0}^{7}Z_{in}\begin{bmatrix}C_n\\S_n\end{bmatrix},\ i \quad 1,2,3 \quad \text{... (20)}$$

After finishing the type (19), the relationship between the end velocity of the manipulator and the angular velocity of each joint was obtained:

$$\dot{P}=\begin{bmatrix}\dot{p}_r\\\dot{p}_l\end{bmatrix}=J^*\dot{\phi}_m \quad \text{... (21)}$$

About the inspection robot arms with six degrees of freedom generalized Jacobian matrix represents J^* $R^{4\ 6}$. When the robot is in a non-normal position, the generalized inverse of J^* can be regarded as. Since $J^*=BC$ is the maximum rank decomposition of J^*, it is available to:

$$(J^*)^+=C^T(CC^T)^{-1}(B^TB)^{-1} \quad \text{... (22)}$$

After synthesis, the dynamic mathematical model of the inspection robot is as follows:

$$M\ddot{q}+C=\tau-J^TF \quad \text{... (23)}$$

M is a symmetric positive definite inertia matrix, C is the

brother's force and the centripetal force is the force of J matrix, generalized Jacobi matrix of the robot end effector, F is the end effect of generalized force on an object, t is the joint driving torque, joint position vector q.

3. Visual design

The inspection robot vision system is used to detect the cracks in the mine rock in the mining process, the camera uses the CCD sensor, its overall design is: the camera image data collected by the LVDS level after the conversion to FPGA cache controller, FPGA controller through the USB2.0 interface to send data to the computer, and then use the LabVIEW JetBrains and PyCharm 5.0.3 visual development programme of image processing and alarm function.

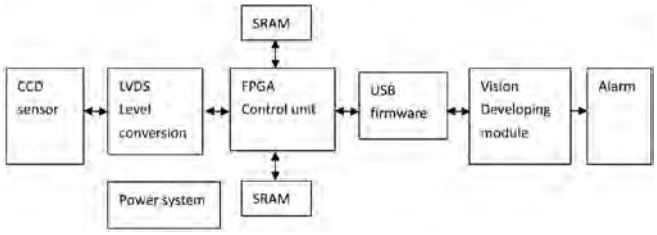

Fig.4 Schematic visual design

4. Binary filtering algorithm for mine image processing

Firstly, carry out the gray image binary processing, then, the image of the crack in the mine tunnel is collected and visual processed by the camera of the robot. The image of the crack in the mine tunnel must be processed by the binary image of the gray level image after the visual processing of the robot. The effect and treatment mainly by the binarization method determines the local threshold method, by comparing global threshold histogram shows Shuangfeng effect in case of disturbances and better use more, but there are also some problems, such as complex algorithm, the speed is not quick, easy in the noise situation in the background region as artifacts, which makes the tunnel crack image processing algorithm which can adapt to the need of non-uniform illumination and effective denoising, the computational efficiency is generally high local threshold method of image binarization method. Therefore, this paper proposes a new algorithm of adaptive filtering with local threshold binarization together, a new adaptive binarization filter design for mine tunnel cracks can make the gray image, because the noise exists distortion of the binarization image information, reduction by way of filtering, so as to realize the image binarization approach the ideal value, improve the accuracy of mine inspection robot to crack judgment and warning. The validity of the new algorithm is proved by experiments.

4.1. Design of adaptive binarization filter

The pixels can be $I*J$ of the mine tunnel gray image $x(i, j)$ as the ideal binary image $c(i, j)$ and distortion noise. An adaptive binarization filter is designed for an image, which is obtained by adaptive filtering of the original image $x(i, j)$, and then the binarization image $y(i, j)$ which is close to the ideal is obtained.

Firstly, the filter formula of the binary image is obtained:

$$y(i,j) = \sum_{m=-N}^{N} \sum_{n=-N}^{N} W_k(m,n)x(i+m,j+n) \quad \ldots (24)$$

Using Otsu algorithm calculate the point of binarization threshold thresh (i, j), $y(i, j)$ binarization, get the ideal binary of two images of C (I, J) of the estimated binary of C (I, J), the instantaneous cost function f (I, J) is defined as:

$$f(i,j) = \mathcal{e}^2(i,j) \quad \ldots (25)$$

Filter error definition:

$$e(i,j) = \hat{C}(i,j) - y(i,j) \quad \ldots (26)$$

Then use the SPGD algorithm to find the minimum value of $f(i, j)$, with the steepest gradient descent method in the LMS algorithm, according to the algorithm, the weight matrix and the noise power is proportional to the negative gradient variable is equal to the weight matrix point, the adjustment formula for weight matrix is:

$$W_{k+1}(m,n) = W_k(m,n) + 2\_e(i,j)x(i+m,j+n) \quad \ldots (27)$$

In the formula W_{k+1} updated weight matrix

W_k not updated weight matrix

Convergence factor, it is a long parameter to control the convergence speed and stability, in order to ensure the stability of the system, must meet formula (28)

$$0 < \_ < \frac{2}{3\,tr\{Rxx\}} \quad \ldots (28)$$

Binary of the pixel processing flow, is shown in Fig.5.

4.2. The local binarization threshold is selected by the improved algorithm of the largest class variance

With the Otsu criterion as the optimal threshold standard, avoids the calculation between group variance and within group variance in the gray level, the gray level histogram of pixel gray level zero points can be excluded from the candidate threshold, the Otsu threshold can be judged only.

where $H(i) = 0 i(i \in [0, L])$ are used as the zero point in the histogram, then the histogram of the zero point distribution mode has the following 3:

(1) There is an integer P satisfying $0 \le p \le L, H(p) \ne 0$ when i = 0,…, p-1, $H(i)$ = 0, when determining the reference area that contains the background and target points, since these points can be divided into one group, the other group of pixels is zero, for any one of the zeros of [0, p-1] is not the best threshold point, so these zeros cannot be a candidate threshold point, so it does not calculate the variance between the two groups.

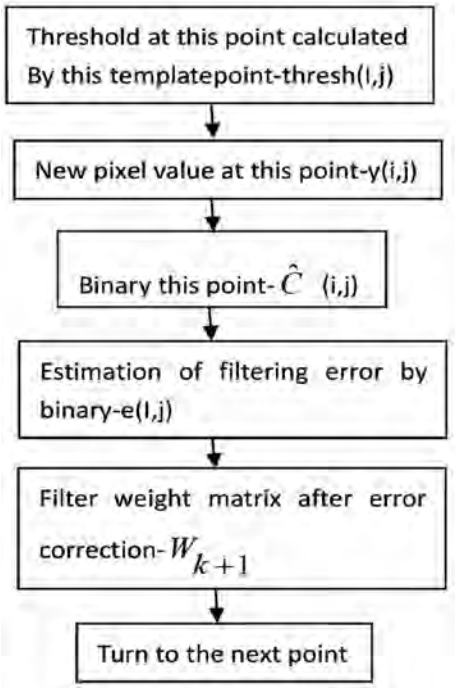

Fig.5 Two flow chart of adaptive filtering 5 valued processing

(2) There is an integer p, q, meet $H(p)\neq 0$, $H(q)\neq 0$, $0\le p\le q\le L$, when $i=p+1,\ldots,q-1, H(i)=0$, the variance between groups can be obtained by the group variance $e_B^2=k_1k_2(M_1-M_2)$, with p, p+1, …, q-1 for Packet Threshold.

$$e_B^2(p)=e_B^2(p+1)=\cdots=e_B^2(q-1) \quad \ldots (29)$$

From [p+1, q-1] served as a point as a threshold point P as threshold for the regional binarization effect is the same, so long as will p points as candidate threshold points can be, [p+1, q-1] in the region can no longer as any zero threshold.

(3) The integer p satisfying $H(p)\neq 0$, when i = p+1,… , L, region [p+1, L] in any one point for the threshold group, a group of pixels is zero, the other group of pixels is the local region of all pixel points, this grouping is similar to the first case, so these zeros can also be excluded from the candidate threshold. If the optimal threshold standard for the maximum and minimum variance between groups within group variance, and ensure that the study area contains the background point and target point, regardless of the position of zero histogram, can be excluded from the candidate threshold, only to calculate the histogram threshold for non-zero packet between group variance to find the best threshold.

4.3. Image processing results of the cracks in the lower strata of the mine

Experiments using 5*7 filter window, then the filter weight matrix of 5*7 matrix. Assuming that the initial filter weights

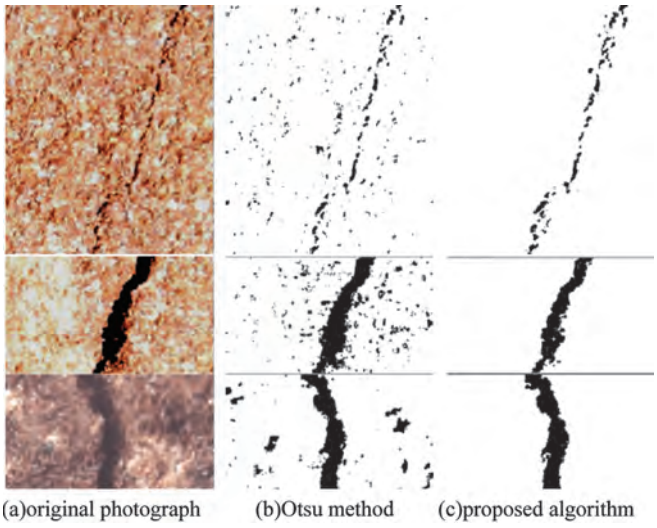

Fig.6 Comparison of experimental results

are: W_o(i, j) = 0.04, I = 1,2,3,4,5; j = 1,2,3,4,5,6,7, the convergence factor is assumed to be :_= 10^{-11}, image edge using zero padding method. Figure 6 is the result of the traditional algorithm with the largest class of variance and the use of this algorithm and the use of different size templates and remove the weights of the binarys obtained after the correction of the results. From the point of view of the value of two, the binary of the image is better than the traditional algorithm based on the improved algorithm.

5. Conclusion

(1) Aiming at the main factors of mine tunnel safety during operation, because the gas and rock burst before the formation of a sudden accident, robot technology and computer vision based design of a mine inspection robot model can replace the manual inspection, and can carry on the tunnel rock crack identification and early warning.

(2) Completed the dynamic modelling of the inspection robot by the dynamic analysis and the mixed model calculation.

(3) The overall design of the visual system for detecting the cracks produced by the mine rock in the mining process is completed by the inspection robot.

(4) The poor image in rock cracks, combined with adaptive filtering with local threshold binarization, based on adaptive filter image binarization, the binarization results to estimate the filtering error and adjust the filter parameters, overcome the influence of shadow and other noise. Through the experiment, it is proved that the binary of the image is better than the traditional algorithm in the local threshold selection, and the value of the image is better than the traditional algorithm.

(5) The improved Otsu algorithm based on visual image processing is used to calculate the threshold at each point to further study the direction of improvement is the reduction of calculating threshold.

Continued on page 290